Supplementary Material for

Inflammation induced repression of Foxp3-bound chromatin in regulatory T cells

Aaron Arvey*[1,2], Joris van der Veeken*[1,2], Robert M. Samstein*[1,2], Yongqiang Feng[1,2], John A. Stamatoyannopoulos[4], Alexander Y. Rudensky[1.2,3]

[1]Howard Hughes Medical Institute, [2]Immunology Program, [3]Ludwig Center, Memorial Sloan-Kettering Cancer Center, New York, NY 10065; [4]Department of Genome Sciences, University of Washington, 1705 NE Pacific Street, Seattle, WA 98195, USA

Corresponding author, rudenska@mskcc.org

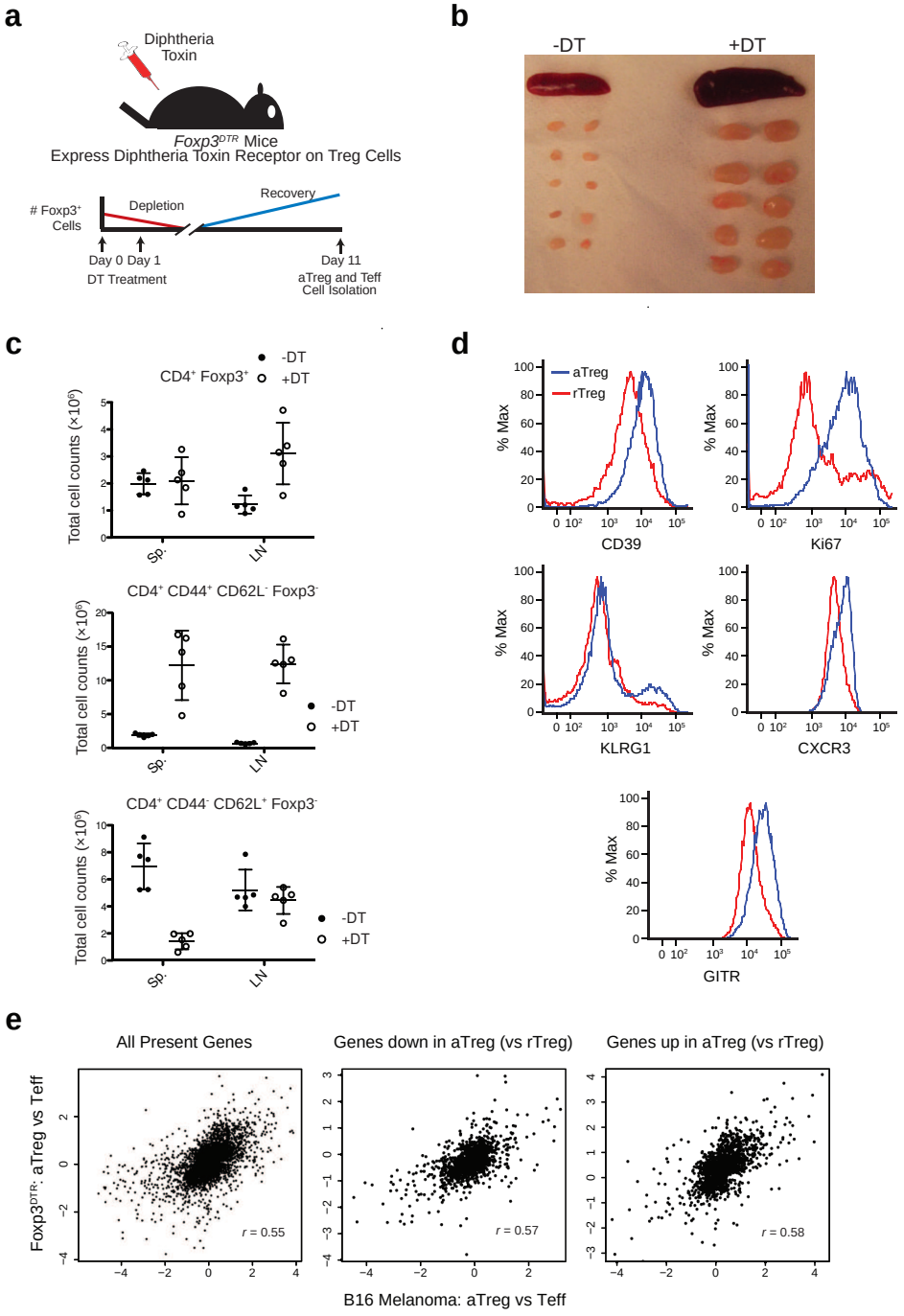

Supplementary Figure 1: Characterization of in vivo activated Treg cells. (**a**) Schematic of generation of in vivo activated Treg and Teff cells. The time course of DT administration to *Foxp3*$^{\mathrm{DTR}}$ mice and subsequent rebound of Treg cells are shown. (**b**) DT-treated mice display splenomegaly and lymphadenopathy (representative of $n > 5$ experiments, each with $n > 3$ DT treated and $n > 3$ untreated *Foxp3*$^{\mathrm{DTR}}$ mice). (**c**) DT-treatment results in increased numbers of Foxp3^{+} Treg and Teff cells on day 11. (**d**) Cell surface effector molecules and proliferation markers are increased in aTreg cells (representative of $n = 3$ experiments, each with $n > 3$ mice). (**e**) Activated Treg cells isolated from diphtheria toxin treated *Foxp3*$^{\mathrm{DTR}}$ mice are representative of activated Treg cells in other inflammatory settings. Intra-tumoral Treg and Teff cells were flow cytometry sorted from B16 melanoma tumors established in *Foxp3*$^{\mathrm{GFP}}$ mice. Gene expression datasets were compared for tumor infiltrating Treg vs. Teff cells (x-axis) and aTreg vs. Teff cells isolated from DT-treated *Foxp3*$^{\mathrm{DTR}}$ mice (y- axis). Plots show all genes called as present (left), those that are expressed at a lower level in aTreg compared to rTreg cells (center), and those that are expressed at a higher level in aTreg cells compared to rTreg cells (right). Pearson correlation values are shown. Tumor Treg and Teff array analysis was performed using two biological replicates.

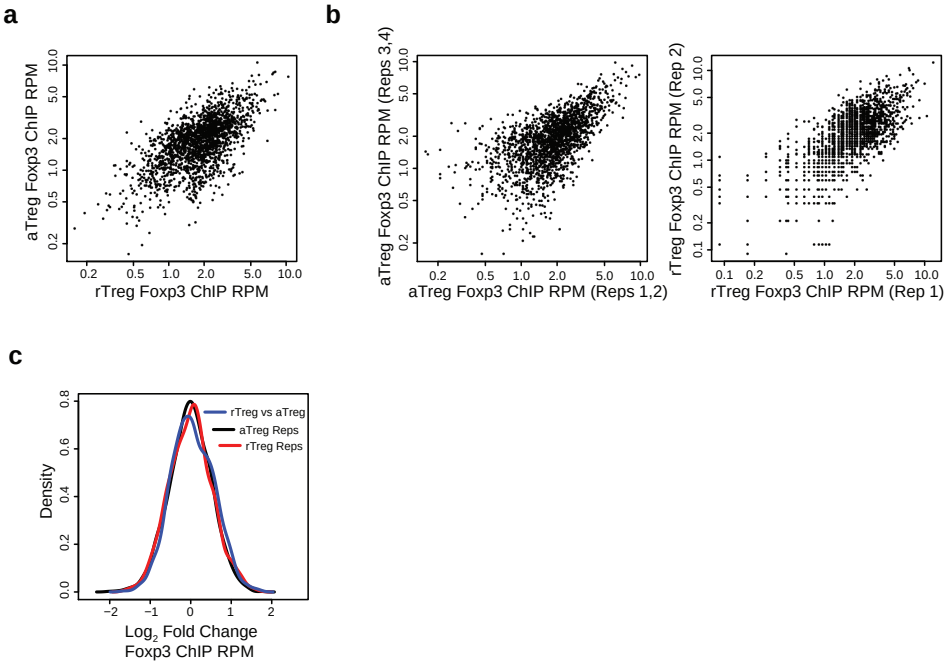

Supplementary Figure 2: Foxp3 binds similar loci in rTreg and aTreg cells and acts predominantly as a repressor. (**a**) Quantitative assessment of Foxp3 ChIP in resting and activated Treg cells. Peaks were called in both resting and activated cells and RPM was computed in each condition on the union of peaks. Data was quantile normalized prior to averaging across $n = 4$ aTreg and $n = 2$ rTreg replicates. Raw data were also analyzed by negative binomial modeling as described in main text and methods. (**b**) Same as A, except x- and y-axes show replicate-to-replicate variation for aTreg (left) and rTreg (right) Foxp3 ChIP-seq RPM data. This analysis demonstrates that the variation observed in A does not surpass reproducibility variation. (**c**) Analysis of the distribution of RPM-fold changes shows that the rTreg-vs-aTreg comparison does not surpass that observed in reproducing the data in either condition.

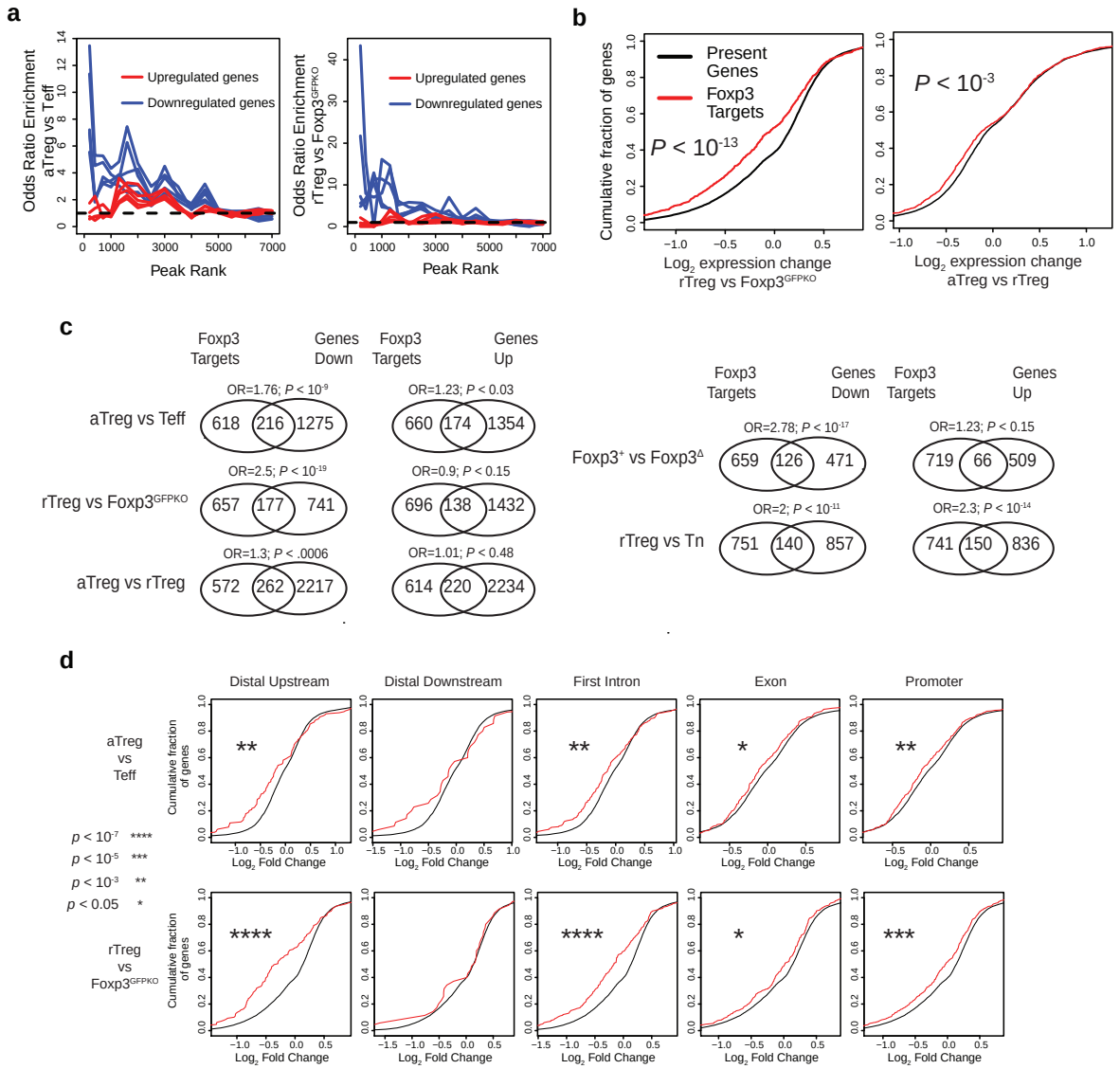

Supplementary Figure 3: (**a**) Peak-rank enrichment of Foxp3 binding for differentially expressed genes. Down- and up-regulated gene sets (blue and red, respectively) are shown at various q-value cutoffs. The y-axis shows the odds ratio of enrichment of the hypergeometric test to estimate the extent of overlap between differentially expressed genes and Foxp3 target genes. (**b**) Cumulative distribution of Foxp3 target gene expression changes in rTreg vs. Foxp3$^{\mathrm{GFPKO}}$ and aTreg vs rTreg cells. (**c**) Overlap of differentially expressed genes with Foxp3 bound genes. Experimental conditions are described in the main text. Odds-ratio (OR) enrichment value and hypergeometric p-values are shown. (**d**) Foxp3-binding at distal upstream and first-intron sites is associated with increased repression of Foxp3-target genes. Cumulative distribution (y-axis) of Log2 expression fold change (x-axis) for aTreg vs Teff cells (top row) and rTreg vs Foxp3$^{\mathrm{GFPKO}}$ cells (bottom row).

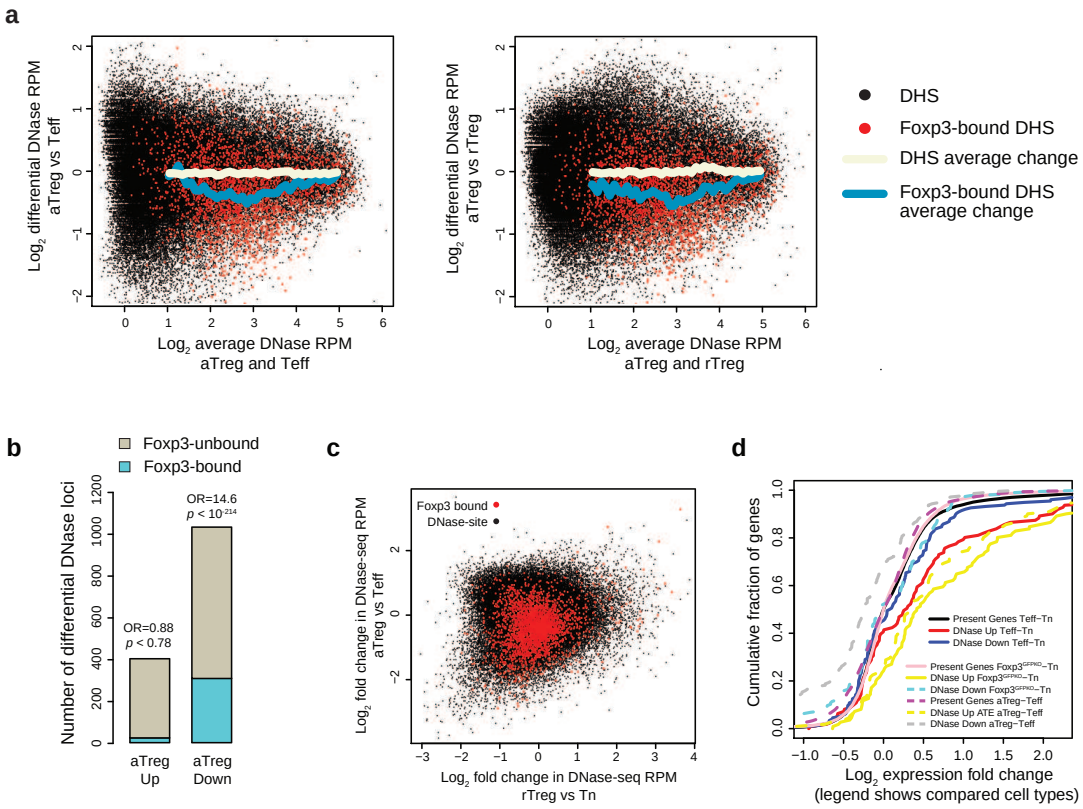

Supplementary Figure 4: Foxp3 bound enhancers are associated with decreased DNase-accessibility. (**a**) Foxp3 association with changes in DNase-accessibility is uniform across average locus accessibility. Lines show running average of fold change (y-axis) relative to total accessibility DNase-seq RPM (x-axis). (**b**) DHSs with decreased accessibility are enriched for Foxp3 binding. This plot represents the same dataset shown in **Fig. 4c** except for the inclusion of DHSs with $q < 0.05$ instead of $q < 0.01$ in **Fig. 4c.** (**c**) DHSs that are Foxp3-bound (shown in red) have decreased chromatin accessibility in aTreg vs. Teff cells (y-axis) that are not repressed in rTreg vs. Tn cells (x-axis). (**d**) Genes near loci with increased DNase accessibility are frequently upregulated in a Foxp3-independent manner. In contrast, many Treg-specific decreases in chromatin accessibility are uniquely associated with Foxp3-dependent decreases in nearby gene expression.

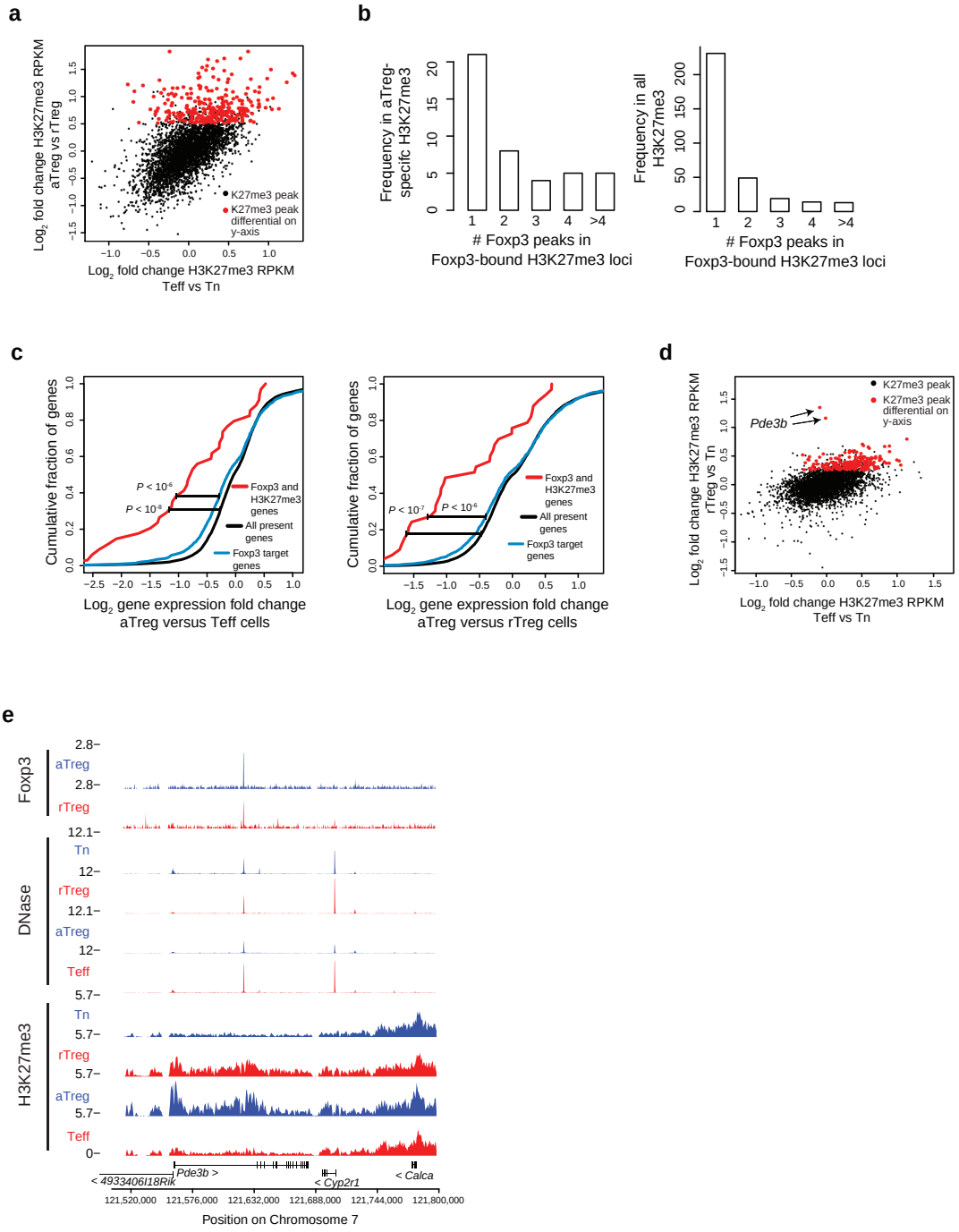

Supplementary Figure 5: (**a**) Activation signals cause changes in H3K27me3 in both aTreg (y-axis) and Teff cell populations (x-axis) relative to their resting counterparts as well as aTreg-specific tri-methylation at a sizable number of loci. (**b**) Histograms demonstrate that a larger fraction of aTreg specific H3K27me3 blocks (left) have multiple Foxp3 binding sites compared to all H3K27me3 blocks (right) ($p < 0.02$, KS-test). (**c**) Decreased expression of Foxp3 target genes with aTreg cell specific increases in H3K27me3. Gene expression changes (x-axis) in aTreg cells compared to Teff (left) and rTreg (right) cells show that Foxp3-bound genes with H3K27me3 (red) have significantly lower expression than those genes that are called as present (black) or are only bound by Foxp3 without increases in H3K27me3 (blue). P values shown are estimated by KS-tests. (**d**) The H3K27me3 landscape of rTreg cells (y-axis) is largely established in a Foxp3-independent fashion in Teff cells (x-axis). (**e**) The *Pde3b* locus contains a Foxp3-bound enhancer that is decreased in accessibility and enriched for H3K27me3.

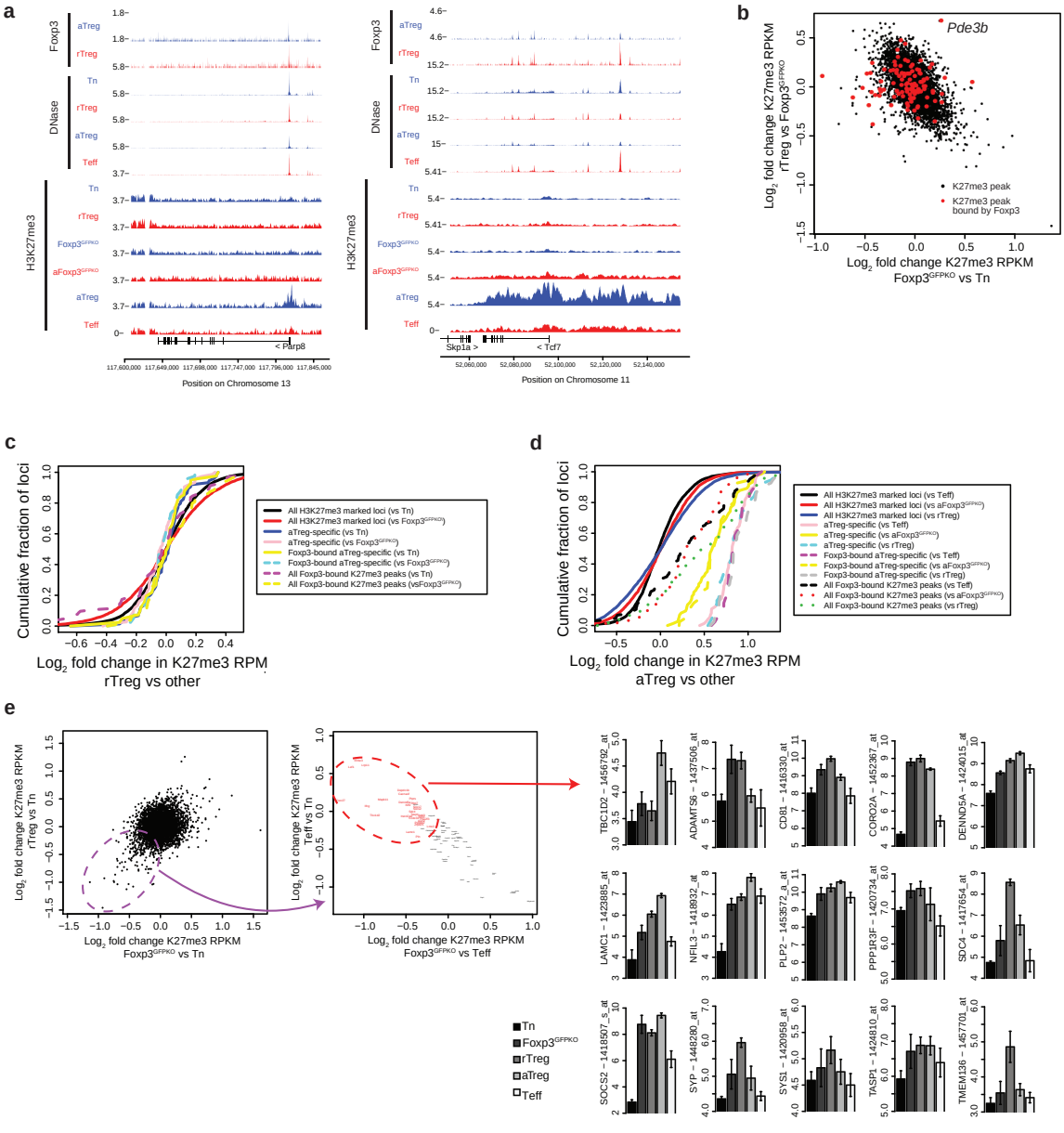

Supplementary Figure 6: (**a**) Tracks showing dependence of aTreg H3K27me3 on Foxp3 at the Parp8 (left) and Tcf7 (right) gene loci. Repressed chromatin is present in aTreg cells, but not in any other population, with the most notable being activated Foxp3^{GFPKO} cells isolated from inflammatory conditions and expressing Foxp3 reporter null allele. (**b**) H3K27me3 at the Pde3b locus in rTreg cells is dependent on Foxp3. (c, d) aTreg cell-specific H3K27me3 is Foxp3 dependent. Quantification of H3K27me3 changes in rTreg vs. other cell type (**c**) or aTreg vs. other cell type (**d**) at Foxp3-bound loci and genome wide. The increase in K27me3 is dependent on Foxp3 (as shown in the comparison to aFoxp3^{GFPKO}) and only in inflammatory conditions. (**e**) Treg lineage specific decreases in H3K27me3 marks are not dependent on Foxp3 and can be found in Foxp3^{GFPKO} cells (left), but not in Teff cells (center) and these genes are upregulated in Treg and Treg precursor Foxp3^{GFPKO} cells (right).

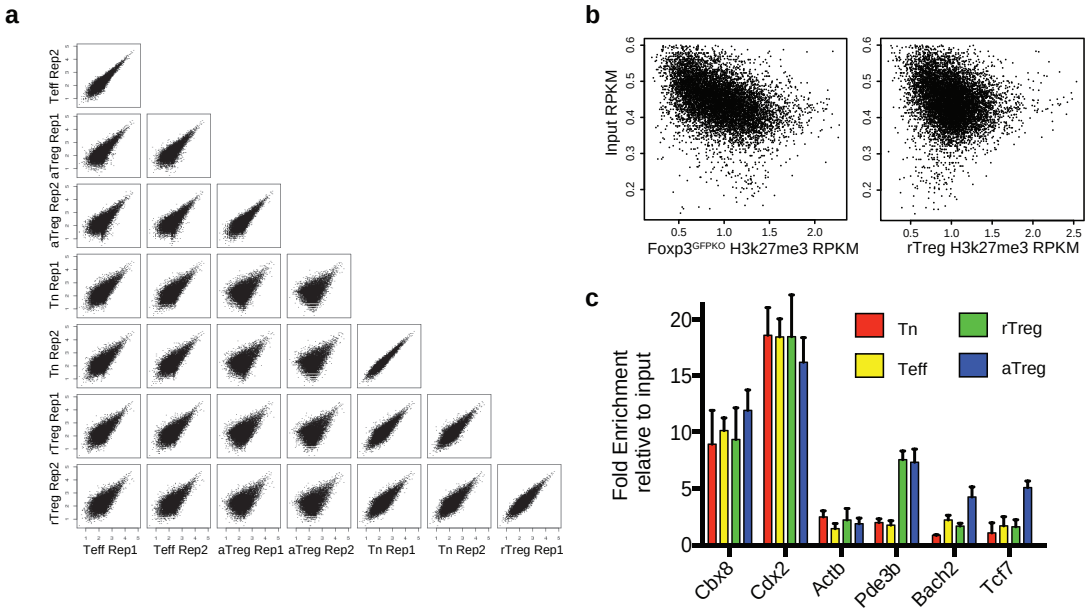

Supplementary Figure 7: (**a**) Distribution of H3K27me3 peaks is highly reproducible between replicates. (**b**) Selection of H3K27me3 peaks. Two representative H3K27me3 ChIP-seq experiments (x-axes) are shown relative to input ChIP-seq (y-axis). H3K27me3 ChIP peaks with fewer reads (e.g. those with RPKM < 0.75) are more likely to be caused by high input signal rather than genuine binding of modified histones. A Poisson test was used to test for statistical enrichment of reads in H3K27me3 peaks with $p < 10^{-7}$ set as a cutoff. (**c**) ChIP-qPCR validation of common and differential H3K27me3 peaks. Experiment done in triplicate.

Supplementary Table Legends:

Supplementary Table 1. Gene expression data for all samples and replicates.

Supplementary Table 2. Normalized RNA expression of genes that are differentially expressed as shown in the **Fig. 1** heatmap.

Supplementary Table 3. Quantification of Foxp3 binding in resting and activated Treg cell ChIP-seq replicates. Values represent units of log2(x+0.5) reads per million.

Supplementary Table 4. The expression change of Akt response genes in Treg cells. Akt response genes are identified based on the deposited gene expression array data (GEO accession GSE7596).

Supplementary Table 5. Quantification of chromatin accessibility. The data are shown as DNase-seq log2(x+0.5) reads per million.

Supplementary Table 6. Quantification of H3K27-tri-methylation. The data are shown as reads per thousand per million.